Available online at www.sciencedirect.com
SCIENCE DIRECT®
Journal of Solid State Chemistry 179 (2006) 500–511
JOURNAL OF SOLID STATE CHEMISTRY
www.elsevier.com/locate/jssc

Structure and magnetic properties of the orthorhombic $n = 2$ Ruddlesden–Popper phases $Sr_3Co_2O_{5+\delta}$ ($\delta = 0.91$, 0.64 and 0.38)

L. Viciu[a,*], H.W. Zandbergen[b], Q. Xu[b], Q. Huang[c], M. Lee[d], R.J. Cava[a]

[a]Department of Chemistry, Princeton University, Princeton, NJ 08540, USA
[b]Department of Nanoscience, Delft Institute of Technology, National Centre for HREM, Al Delft, The Netherlands
[c]NIST Center for Neutron Research, NIST, Gaithersburg, MD 20899, USA
[d]Department of Physics, Princeton University, Princeton, NJ 08540, USA

Received 19 September 2005; received in revised form 28 October 2005; accepted 3 November 2005
Available online 20 December 2005

Abstract

The reduced Ruddlesden–Popper phases, $Sr_3Co_2O_{5+\delta}$ with $\delta = 0.91$, 0.64 and 0.38, have been prepared in a nitrogen atmosphere. The crystal structures were determined by powder neutron diffraction. Oxygen vacancies are found both in O(3) and O(4) sites but the majority are along one crystallographic axis in the CoO_2 plane, inducing an orthorhombic distortion of the normally tetragonal $n = 2$ Ruddelsden–Popper structure. Superstructures due to oxygen ordering are observed by electron microscopy. The magnetic measurements reveal complex behavior with some ferromagnetic interactions present for $Sr_3Co_2O_{5.91}$ and $Sr_3Co_2O_{5.64}$.

Keywords: $Sr_3Co_2O_{5+\delta}$; Oxygen deficient Ruddlesden–Popper phase; Magnetic properties

1. Introduction

The recent discovery of superconductivity in the layered hexagonal structure of $Na_{0.3}CoO_2 \cdot 1.3H_2O$ [1], has prompted a search for new materials based on cobalt and oxygen that might exhibit unexpected properties. The appeal of cobalt-based compounds comes from the richness of available cobalt oxidation states and cobalt's ability to display more than one spin state within a structure, leading to intriguing competing phenomena. The mixed oxidation state of Co^{3+}/Co^{4+} in $Na_{0.3}CoO_2$, in which cobalt has a low spin configuration, is believed to play an essential role in its superconductivity [2].

This mixture of Co^{3+}/Co^{4+} is also found in perovskites, $Ln_{1-x}Sr_xCoO_3$ [3] and $LnBaCo_2O_{5+\delta}$ [4], with Ln = lanthanides. In the oxygen deficient perovskites, $LnBaCo_2O_{5+\delta}$, the Ba and Ln ions order in alternating (001) planes of a tetragonal structure with oxygen vacancies situated in the $LnO_{0.5}$ layer. This vacancy ordering generates both square-pyramidal and octahedral sites for cobalt. Of most interest in this family are the compounds with $\delta = 0.5$ where the cobalt ions are in a single valence state (3+) equally distributed between octahedra and pyramids. At high temperatures, both pyramidal and octahedral Co^{3+} ions are in the high spin state ($t_{2g}^3 e_g^2$) [5]. At low temperatures, the octahedral Co^{3+} ions are found in low spin state $\left(t_{2g}^6\right)$ whereas the square pyramidal Co^{3+} ions are in the intermediate spin state ($t_{2g}^5 e_g^1$) [6]. These different spin states are key to understanding the peculiar way the magnetic and transport properties change with composition and temperature.

Many Ruddlesden–Popper (RP), $A_{n+1}B_nO_{3n+1}$-type structures having 3*d* transition metals on the *B* site have been found. A comparison between iron- and cobalt-based compounds can be drawn due to their similar sizes and potential oxidation states. $Sr_3Fe_2O_7$ is an example of $n = 2$ RP-type phase where iron is in a 4+ oxidation state [7]. It was shown by ^{57}Fe Mössbauer spectroscopy that Fe^{4+} disproportionates to Fe^{3+} and Fe^{5+} around 343 K [8]. RP structures containing only Co^{4+} ions are known for $n = \infty$, $SrCoO_3$ which can be obtained either at high oxygen pressure (200 bar) [9] or by electrochemical oxidation of $SrCoO_{2.5}$ [10] and for $n = 1$ in single crystalline film

*Corresponding author. Fax: +1 609 258 6746.
E-mail address: mviciu@princeton.edu (L. Viciu).

0022-4596/$ - see front matter © 2005 Elsevier Inc. All rights reserved.
doi:10.1016/j.jssc.2005.11.013

Sr_2CoO_4 obtained by the pulsed-laser deposition method [11]. The substitution of iron by cobalt in the system $Sr_3Fe_{2-x}Co_xO_{7-\delta}$ at high oxygen pressures allowed the stabilization of both Fe and Co in the 4+ formal oxidation state [12–18]. However, with increasing Co content, the level of oxygen deficiency was found to increase [18]. In the $n=2$ cobalt only based RP member, $Sr_3Co_2O_{7-y}$, a tetragonal symmetry average structure phase with oxygen stoichiometry ranging from $0.94 \leqslant y \leqslant 1.22$ ($Sr_3Co_2O_{5.78}$ to $Sr_3Co_2O_{6.06}$) has been synthesized in both air and oxygen [19]. For $Sr_3Co_2O_{5.78}$, the coordination number around cobalt is both octahedral and square pyramidal, with the oxygen vacancies ordered along the *b*-axis, causing a $3\times$ supercell in this direction. For $Sr_3Co_2O_{6.06}$, the oxygen vacancies are displayed exclusively on the site linking the CoO_6 octahedra within the perovskite layers in the RP block, and the geometry around the cobalt is square pyramidal.

Here we show that the range of oxygen stoichiometry in the $n=2$ RP phase can be extended to considerably lower oxygen contents by synthesis in nitrogen, forming a distinct series of orthorhombic compounds of the type $Sr_3Co_2O_{5+\delta}$. Unlike what is found in an oxygenated atmosphere, a different ordering pattern of the oxygen vacancies occurs. A substantial number of vacancies are found in the CoO_2 planes themselves, with a strong preference for vacancies to occur along one of the in-plane directions. This induces a strong orthorhombic distortion, resulting in one very short in-plane dimension (about 3.6 Å). This phase can be transformed into the previously reported tetragonal phase synthesized under oxidizing conditions by annealing in a controlled oxygen ambient at low temperature. Measurements of the magnetic properties of $Sr_3Co_2O_{5+\delta}$ show that they are sensitive to the Co^{2+}/Co^{3+} ratio as well as to the fashion in which the oxygen vacancies order. With nearly the same compositions in the intermediate oxygen content region, the $n=2$ $Sr_3Co_2O_x$ ($x=5+\delta$ and $7-y$) phases prepared in oxidizing and reducing ambients are an excellent example of a system that displays distinctly different structure and properties at one overall composition due only to the arrangement of the oxygen vacancies.

2. Experimental

The starting materials $SrCO_3$ (Alfa, 99.99%) and Co_3O_4 (Alfa, 99.7%) were mixed together in the molar ratio Sr:Co = 3:2. After thoroughly grinding, the mixture was pressed into a pellet ($\varnothing = 0.8$ cm) and annealed under flowing nitrogen (approximately 10^{-4} atm O_2 in our apparatus) at 800 °C for 24 h. The temperature was then increased to 1050 °C and held constant for another 24 h. The oxygen stoichiometry and vacancy ordering were determined by the cooling rate. At lower cooling rates, more oxygen was absorbed by the compounds when cooling from 1050 °C to room temperature at low oxygen pressure. Thus, the cooling rate allowed by the furnace (approximately 6 °C/min) gives $Sr_3Co_2O_{5.91}$. Quenching the material from 1050 °C under nitrogen was found to result in two other different oxygen contents, $Sr_3Co_2O_{5.64}$ and $Sr_3Co_2O_{5.38}$. Control of oxygen content through quenching alone could not be reproducibly established because the cooling rate was not well controlled. $Sr_3Co_2O_{5.64}$ could be obtained reproducibly by quenching, but $Sr_3Co_2O_{5.38}$ was difficult to obtain by this method. Rather it was found that thermal treatment of $Sr_3Co_2O_{5.64}$ at 300 °C for 36 h under flowing hydrogen resulted in the formation of $Sr_3Co_2O_{5.38}$, and this process was used to make this compound. The compounds are found to be stable in atmospheric conditions.

All samples were analyzed by powder X-ray diffraction using CuKα radiation and a diffracted beam monochromator. The oxygen content was solely determined from neutron diffraction analysis. Neutron diffraction data were collected on each sample at the NIST Center for Neutron Research on a high-resolution powder neutron diffractometer with monochromatic neutrons of wavelength 1.5403 Å produced by a Cu(311) monochromator. Collimators with horizontal divergences of 15′, 20′ and 7′ of arc were used before and after the monochrometer and after the sample, respectively. Data were collected in the 2θ range of 3–168° with a step size of 0.05°. The structural parameters were refined using the program GSAS [20]. The neutron scattering amplitudes used in the refinement were 0.702, 0.253 and 0.581 (10^{-12} cm) for Sr, Co and O, respectively.

Electron transparent areas of the specimens were obtained by crushing them under ethanol to form a suspension and then dripping a droplet of this suspension on a carbon-coated holey film on a Cu grid. Electron microscopy analysis was performed with Philips CM200ST and Philips CM300UT electron microscopes having field emission guns and operated at 200 and 300 kV, respectively. The magnetic susceptibilities were measured with a Quantum Design PPMS system. Zero field cooled (ZFC) and field cooled (FC) magnetic data were taken between 5 and 280 K in an applied field of 1 T. Hysteresis data were recorded at 5, 100, and 170 K. A dc four-probe method was used to measure the resistivity of the samples in the 210–290 K temperature range.

3. Results and discussion

As described above, when $SrCO_3$ is reacted with Co_3O_4 under flowing nitrogen and allowed to cool at different rates, the formation of different oxygen compositions of formula $Sr_3Co_2O_{5+\delta}$ with $\delta = 0.91$, 0.64 and 0.38 was obtained. All these compounds have the same orthorhombic average structure and have similar powder X-ray diffraction patterns (Fig. 1). Electron diffraction, using a tilt series along the *c*-axis, was performed to estimate the unit cell parameters of these phases. The basic unit cell was found to be *I* centered with $a = 3.9$ Å, $b = 3.7$ Å and $c = 20$ Å and three angles equal or very close to 90°. Accurate

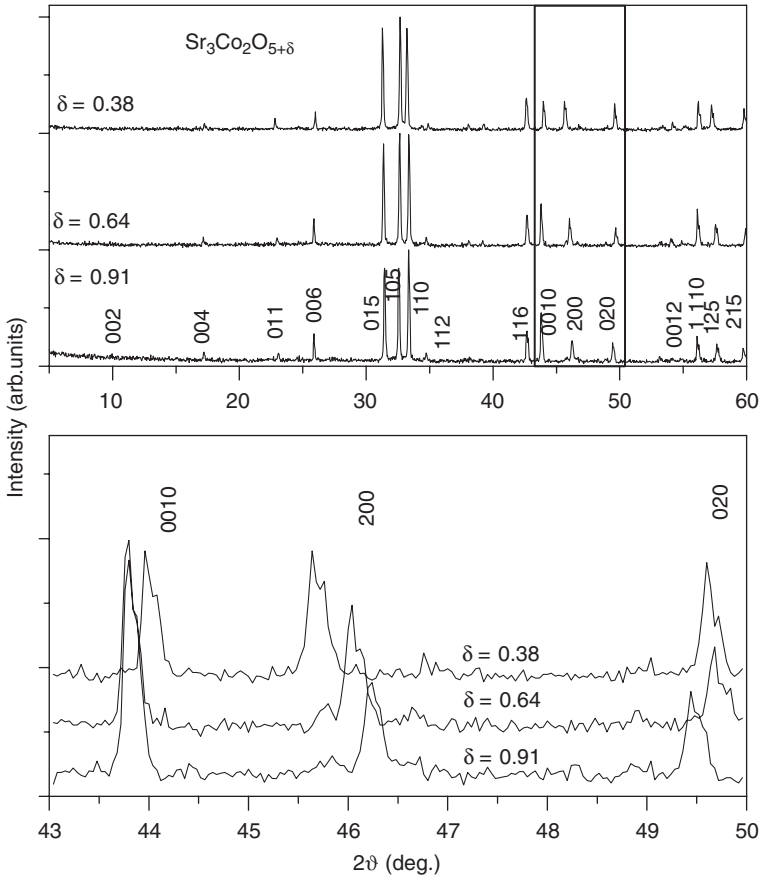

Fig. 1. Top: Powder X-ray diffraction patterns for $Sr_3Co_2O_{5+\delta}$ ($\delta = 0.38$; 0.64 and 0.91); The Miller indices are shown for selected reflections. Bottom: Detail of all patterns in the 43–50° 2θ range.

Table 1
The cell parameters of $Sr_3Co_2O_{5+\delta}$ ($\delta = 0.91$, 0.64, 0.38) at 295 K

δ	a (Å)	b (Å)	c (Å)	V (Å^3)
0.91	3.9261(2)	3.6889(2)	20.6779(9)	299.48(4)
0.64	3.9442(2)	3.6687(1)	20.6810(8)	299.26(4)
0.38	3.9721(2)	3.6753(2)	20.573(1)	300.34(4)

determination of the cell constants was then established from X-ray powder diffraction data. Consequently, all the lines in the patterns were indexed based on a body centered orthorhombic cell. Unit cell parameters for all three compositions are given in Table 1. The cell size varies as the oxygen composition changes. This can be best visualized in the expanded region ($2\theta = 43 - 45^\circ$) of the diffraction patterns in Fig. 1 bottom, where the reflections (0010), (200) and (020) are found. The cell parameters are not changing much from one composition to the other, with the a-axis being the smallest for the most oxygenated sample. This is not surprising considering the difference in ionic radius between Co^{2+} and Co^{3+} since the Co^{2+}/Co^{3+} ratio increases as the oxygen content decreases. The b- and c-axis vary as well, and their sizes correlate to the occupation factor of the oxygen on the O(3) and O(4) crystal sites. Consequently, the c-axis is the smallest for $Sr_3Co_2O_{5.38}$ in which the O(3) site is least occupied. Similarly, the b-axis is the smallest in $Sr_3Co_2O_{5.64}$ where O(4) site is least occupied.

Structural analysis by the Rietveld method on neutron diffraction data was performed for all compositions in a body centered cell (space group *Immm*) considering a RP two-layer structure. The big difference between the a- and b-axis clearly indicated that the oxygen vacancies are found mostly along the short direction of the cell. No extra reflections to account for long-range ordering of the vacancies in the structure could be seen in the neutron diffraction patterns. Therefore, an average structural model was used to fit the data. The refined structural parameters can be found in Table 2. There are two independent Sr ions, one type of Co, and four independent oxygen ions. In the early stages of the refinements, O(2) and O(3) were placed on (0, 0, z) and (0, 0, 0) positions, respectively, with isotropic thermal parameters. A significant improvement of the fit was obtained when anisotropic refinement of the thermal parameters was allowed. The values of the thermal factors for the oxygens in the cobalt plane were still not satisfactory, suggesting displaced disorder of these atoms in to off-center positions. Moving both O(2) and O(3) to more general positions (0, y, z) and

Table 2
Crystallographic data for $Sr_3Co_2O_{5+\delta}$ ($\delta = 0.91, 0.64, 0.38$); space group #71-*Immm* at room temperature

Compound	Atom	Site	x	y	z	Occ.	U_{11}; U_{22}; U_{33} [U_{iso}] ($\times 100$) Å^2
$Sr_3Co_2O_{5.91}$	Sr(1)	2*c*	0.5	0.5	0	1	1.7(2); 3.8(4); 1.5(2)
$wR_p = 5.61\%$	Sr(2)	4*i*	0	0	0.3146(1)	1	2.4(1); 0.8(1); 0.8(1)
$R_p = 4.44\%$	Co	4*i*	0	0	0.1004(3)	1	1.0(3); 1.9(3); 0.6(3)
$\chi^2 = 1.94$	O(1)	4*j*	0.5	0	0.0947(2)	1	4.4(3); 3.2(2); 3.1(2)
	O(2)	4*i*	0	0	0.1953(1)	1	1.2(2); 1.5(2); 1.2(1)
	O(3)	4*i*	0	0	0.0108(4)	0.317(8)	[0.6(3)]
	O(4)	4*j*	0	0.5	0.0847(3)	0.64(1)	5.0(4); 1.8(3); 3.9(3)
$Sr_3Co_2O_{5.64}$	Sr(1)	2*c*	0.5	0.5	0	1	3.2(3); 1.2(2); 1.1(2)
$wR_p = 6.18\%$	Sr(2)	4*i*	0	0	0.3142(1)	1	2.3(2); 1.6(2); 0.7(1)
$R_p = 5.0\%$	Co	4*i*	0	0	0.1002(4)	1	1.7(4); 1.9(3); 1.2(4)
$\chi^2 = 1.47$	O(1)	4*j*	0.5	0	0.0934(2)	1	4.1(3); 2.6(2); 3.0(2)
	O(2)	8*l*	0	0.042(2)	0.1947(2)	0.5	[0.8(1)][a]
	O(3)	4*i*	0	0	0.0104(7)	0.26(1)	[1.3(5)]
	O(4)	4*j*	0	0.5	0.0809(4)	0.56(1)	5.5(5); 0.05(3); 5.1(5)
$Sr_3Co_2O_{5.38}$	Sr(1)	2*c*	0.5	0.5	0	1	2.3(2); 0.9(2); 1.5(2)
$WR_p = 5.6\%$	Sr(2)	4*i*	0	0	0.3150(1)	1	2.3(2); 1.0(1); 1.2(1)
$R_p = 4.5\%$	Co	4*i*	0	0	0.1022(3)	1	1.5(4); 1.2(3); 1.0(3)
$\chi^2 = 1.19$	O(1)	4*j*	0.5	0	0.0881(3)	1	7.0(3); 2.2(2); 3.6(2)
	O(2)	8*l*	0	0.026(3)	0.1964(2)	0.5	[1.0(1)][b]
	O(3)	4*i*	0	0	0.011(2)	0.12(1)	[4(1)]
	O(4)	4*j*	0	0.5	0.0746(3)	0.57(1)	4.4(5); 0.8(3); 2.5(4)

[a] U_{11},U_{22}, and U_{33} are 0.8, 3.3, and 0.8×100 for O(2) at (0, 0, 0.1947), $\chi^2 = 1.665$ for refining with isotropic temperature.
[b] U_{11}, U_{22}, and U_{33} are 1.4, 2.0, and 0.6×100 for O(2) at (0, 0, 0.1964), $\chi^2 = 1.422$ for refining with isotropic temperature factor.

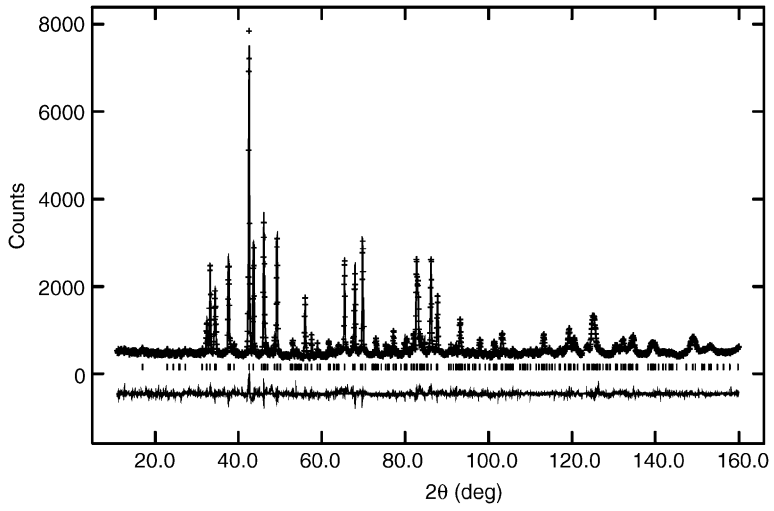

Fig. 2. Observed (crosses) and calculated (solid line) neutron diffraction intensities for $Sr_3Co_2O_{5.91}$ at 295 K. Vertical bars show the Bragg peak positions. The difference plot is shown at the bottom.

(0, 0, z), respectively, found them to indeed be better described in displaced positions, and a substantially better refinement was then achieved. However, in-plane displacement of O(2) in $Sr_3Co_2O_{5.91}$ was not significant, and therefore the atom was left at (0, 0, z). For the O(4) atom, displacements from the ideal position were insignificant for all samples. No deviation from stoichiometry was observed for the Sr, Co, O(1) and O(2) atoms in any of the refinements. Therefore, the occupation factor of these atoms was fixed in the final models. An example of the observed, calculated and the difference plots of the refinement based on this model are presented for $Sr_3Co_2O_{5.91}$ in Fig. 2.

The idealized crystal structure is presented in Fig. 3 and selected bond distances are shown in Table 3. The structure obtained by neutron diffraction averages over all Co–O coordination polyhedra that are present. The O(3) site is found to be less occupied in all three compounds and therefore the predominant cobalt geometry must be pyramidal, though some octahedra may be present. The

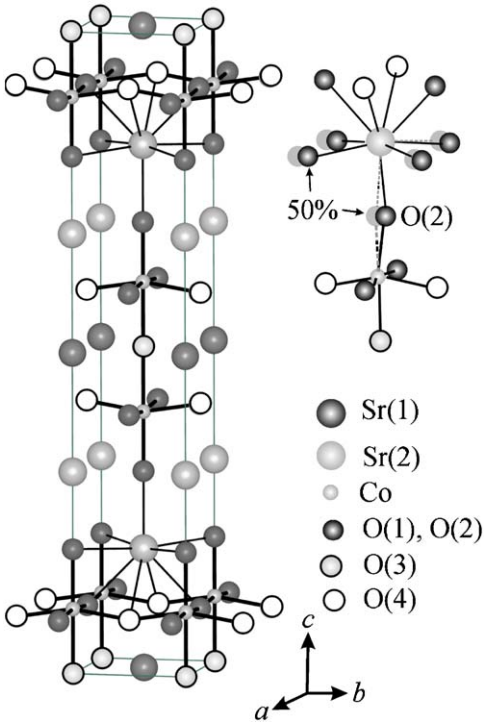

Fig. 3. Idealized structure representation of $Sr_3Co_2O_{5+\delta}$. The right side of the figure shows the displacement of O(2) and how the polyhedra are distorted.

Table 3
Selected bond distances for $Sr_3Co_2O_{5+\delta}$ ($\delta = 0.91$, 0.64 and 0.38) at room temperature

Bonds	Bond distances (Å)		
	$\delta = 0.91$	$\delta = 0.64$	$\delta = 0.38$
Sr(1)–O(1) × 4	2.690(3)	2.664(4)	2.580(4)
Sr(1)–O(3)[a] × 4	2.703(7)	2.702(1)	2.715(4)
Sr(1)–O(4)[a] × 4	2.632(4)	2.587(5)	2.510(3)
Sr(2)–O(1) × 2	2.630(3)	2.648(4)	2.712(4)
Sr(2)–O(2) × 1	2.467(3)	2.478(4)	2.442(4)
Sr(2)–O(2) × 4	2.7015(3)	2.807(5)	2.781(7)
Sr(2)–O(4)[a] × 2	2.860(5)	2.930(6)	3.016(5)
Co–O(1) × 2	1.9666(5)	1.9771(8)	2.007(2)
Co–O(2) × 1	1.963(6)	1.959(8)	1.941(6)
Co–O(3)[a] × 1	1.853(9)	1.86(2)	1.88(5)
Co–O(4)[a] × 2	1.873(1)	1.877(2)	1.923(2)

[a]O(3) and O(4) are partially occupied.

O(4) site is also partially occupied. When O(4) is absent, then we postulate that the coordination around cobalt may be tetrahedral. This geometry can be seen in Fig. 3 if considering the highlighted O(2) position and one of the O(4) sites vacant. In an attempt to achieve maximum energy stabilization of the structure, the CoO_n polyhedra may rotate to accommodate the very short *b*-axis. This makes the oxygen atoms move from their ideal positions and results in large thermal factors for these atoms for the average structure model.

The average formal oxidation states for Co in $Sr_3Co_2O_{5+\delta}$ with $\delta = 0.91$, 0.64 and 0.34 are 2.91, 2.64 and 2.38, respectively. Co^{2+} in five-fold coordination has a radius of 0.67 Å and when bound to oxygen ($r_O^{2-} = 1.40$ Å) gives an expected bond length of ~2.03 Å [21]. Thus, the slightly average larger bond distances seen in $Sr_3Co_2O_{5.38}$ are attributed to the fact that this structure contains the highest percentage of Co^{2+}. Overall, the bond distances are in agreement with what has been previously seen for cobalt in the same geometrical configuration. For instance, in the previously reported tetragonal $n = 2$ RP phase, $Sr_3Co_2O_{7-y}$ ($0.94 \leqslant y \leqslant 1.22$), Co–O bonds of 1.93–2.01 Å are seen [19]. In RP-type cobalt oxychlorides, $Sr_3Co_2O_5Cl$ and Sr_2CoO_3Cl, the CoO_5Cl octahedra have four in-plane Co–O bonds of 1.97 Å and one apical Co–O bond of 1.86 Å[22]. In these phases the Cl^- is found relatively far from Co (Co–Cl = 3.0–3.1 Å) and the cobalt geometry is best described as square pyramidal.

Efforts to model the pattern of vacancy ordering in these structures were made by electron diffraction analysis. The diffraction patterns showed superstructures (Fig. 4) on all individual grains investigated. The [010] diffraction patterns for $Sr_3Co_2O_{5.91}$ (Fig. 4a) and $Sr_3Co_2O_{5.64}$ (Fig. 4b) show superreflections that can be indexed with doubled and tripled *a* axes, respectively. The subcell reflections reflect the *I* centering of the average structure. The superreflections of $Sr_3Co_2O_{5.91}$ show a doubling of *a*-axis and no systematic absences. The superreflections of $Sr_3Co_2O_{5.64}$ show a tripling of the *a*-axis and a tripling of the *c*-axis. Alternatively, one can describe the superstructure reflections with a vector **q** (see Fig. 4), which is $\pm\mathbf{a}^*/2$ for $Sr_3Co_2O_{5.91}$ and $\pm(\mathbf{a}^*-\mathbf{c}^*)/3$ for $Sr_3Co_2O_{5.64}$. The [100] diffraction patterns for both compositions (not shown) show $0\,k\,l$ superreflections with $k = n + 1/2$ (thus indicating a doubling of the *b*-axis). These superreflections are strongly streaked along $\mathbf{c}^*$ indicating imperfect ordering perpendicular to the plane. The electron diffraction studies indicated that the ordering changed over a period of several months.

Attempts to increase the oxygen content beyond 5.91 in the orthorhombic compound were made. When the samples where sealed in a quartz tube ($V \approx 37\,cm^3$) with Ag_2O as an oxygen source and annealed at 325 °C for 12 h, the material became tetragonal $Sr_3Co_2O_{6.06}$. The Ag_2O content of the tube was limited to provide a maximal 1.5 mole oxygen per formula unit. Heating in a richer oxygen ambient at higher temperatures resulted in the formation of $Sr_5Co_4O_{12}$ [23]. As recently reported by Pelloquin et al. [24], $Sr_3Co_2O_{6.06}$ is highly sensitive to atmospheric moisture and becomes an oxyhydrate. The possibility that the product created by exposure of $Sr_3Co_2O_{6.06}$ to air was an oxycarbonate was excluded after performing the following experiment: the obtained $Sr_3Co_2O_{6.06}$ was sealed into two rubber caped vials inside an argon filled glove box; one vial was flushed with

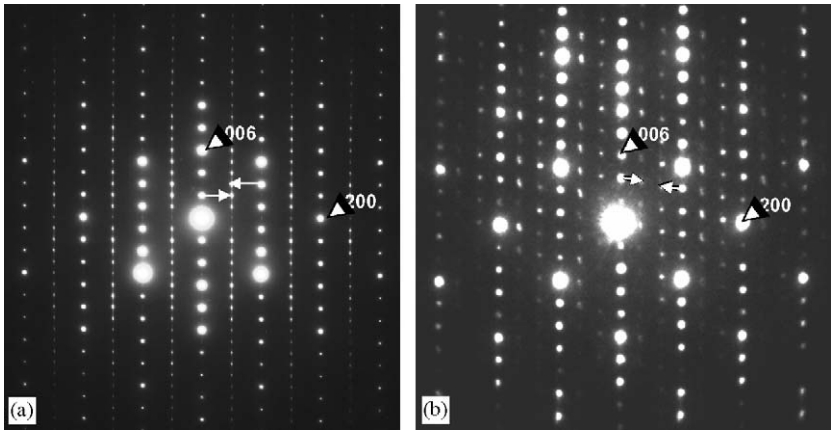

Fig. 4. [010] Diffraction patterns of (a) $Sr_3Co_2O_{5.91}$ and (b) $Sr_3Co_2O_{5.64}$ showing the superstructure along the *a*-axis. The super reflections can be described by a vector **q**, which originates in the main reflections. White arrows in (a) and (b) indicate the vectors **q**.

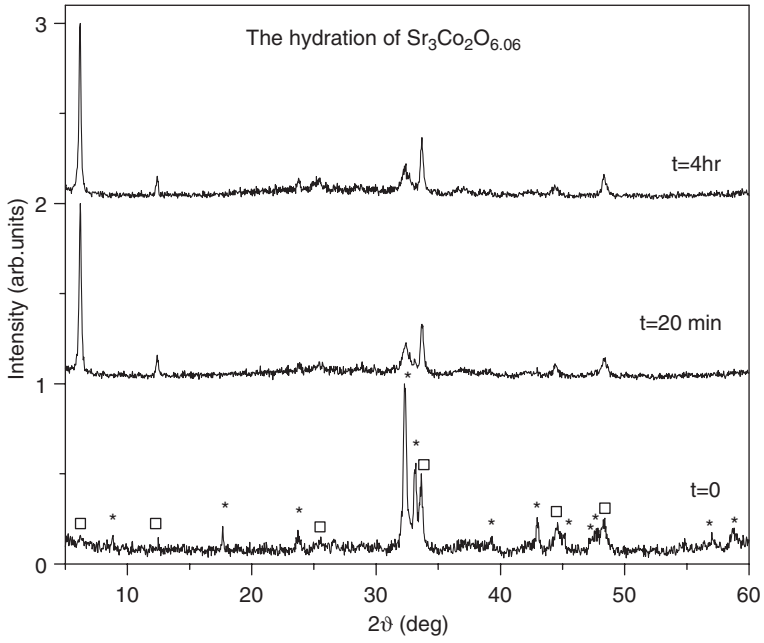

Fig. 5. XRD patterns for the product between $Sr_3Co_2O_{5.91}$ and oxygen (a) taken in air after the pellet was extracted from the sealed tube containing oxidizer; (b) taken after the 20 min scan recorded for (a) was finished; and (c) after 4 h in air. The stars in (a) indicate the lines corresponding to $Sr_3Co_2O_{6.06}$ (tetragonal cell: $a = 3.831(1)$ Å, $c = 20.082(6)$ Å) [7] while the squares are the lines for the hydrated phase.

CO_2 gas and the other one was flushed with argon passing through water. After 24 h of sample exposure to the gases, the vials were stored again in the glove box. The XRD pattern analysis indicated a phase change only for the case where the sample was exposed to argon bubbled through water. In the laboratory air, its *c*-axis changes in less than 20 min, from 20.082(6) to 28.571(2) Å in our measurements (Fig. 5). The XRD pattern of the oxyhydrate material was successfully indexed with a monoclinic cell with $a = 3.7626(3)$ Å, $b = 3.7652(3)$ Å, $c = 28.571(2)$ Å and $\beta = 90.970(9)^\circ$ in very close agreement with the one found by Pelloquin and coworkers. Thermal gravimetric studies were performed on this sample in Ar up to 400 °C (Fig. 6). The data show two major weight losses of approximately the same amount: one of 4.00%, which ends at ~280 °C, due to the loss of water, and the second of 4.11%, which ends around 380 °C and is attributed to the departure of hydroxyl groups [24]. The two distinct weight losses observed in the present study allow for water and hydroxyl group content to be well determined, and we find the chemical formula of this material to be $Sr_3Co_2O_5(OH)_{1.2} \cdot 1.2(H_2O)$. There is no color change on formation of the hydrate. Analogous behavior has been noticed for the $n = 2$ RP analogue, $Sr_3Fe_2O_{7-\delta}$, which intercalates 1.8 water molecules [25]. In this case, the *c*-axis expands by ~7.8 Å. It seems that these materials, which have as a common

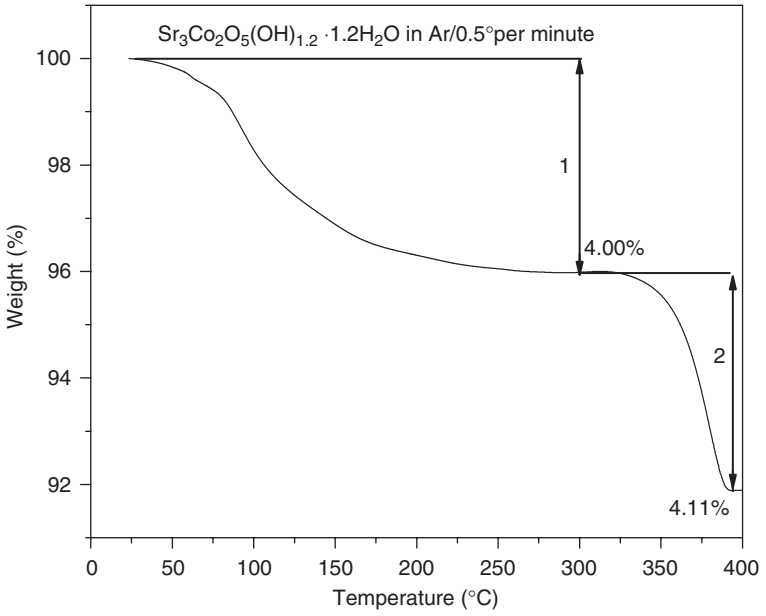

Fig. 6. TGA analysis on heating in an Ar atmosphere of the hydroxyhydrated phase, $Sr_3Co_2O_5(OH)_{1.2}\cdot 1.2(H_2O)$.

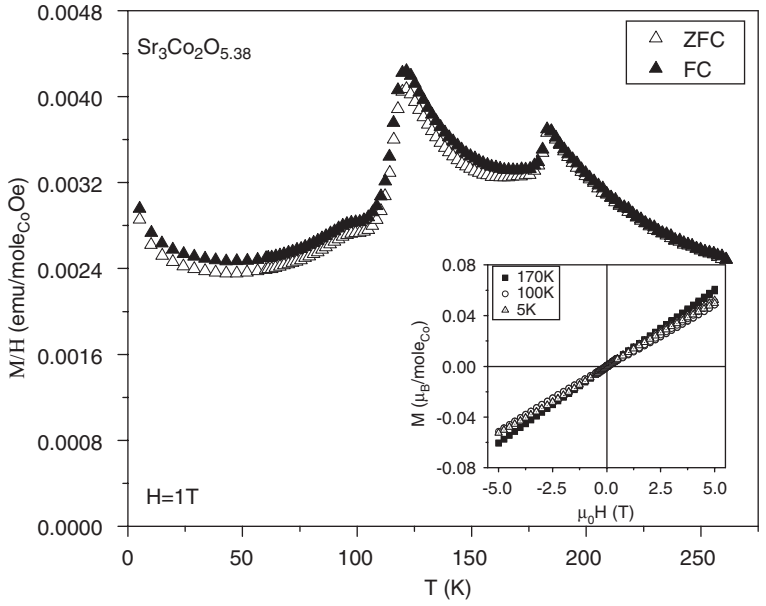

Fig. 7. Temperature dependence of magnetic susceptibility for $Sr_3Co_2O_{5.38}$. The inset shows the magnetization vs. applied field at 5, 100 and 170 K.

feature oxygen deficiency in a layered structure, have the tendency to stabilize their structure by accommodating water molecules and hydroxyl groups.

Magnetic susceptibility data for all samples were recorded in an applied field of 1 T. Their magnetic behavior is rather complex. The ZFC/FC data for $Sr_3Co_2O_{5.38}$ are presented in Fig. 7. The high temperature data from the ZFC curve, from 190 to 260 K, were fit with the Curie–Weiss law, giving an effective magnetic moment $\mu_{eff} = 1.13\,\mu_B$ and a Weiss constant $\theta = -28$ K. The value of Weiss constant indicates antiferromagnetic (AFM) interactions. At lower temperature, two sharp transitions are observed, with their maxima at 185 and 120 K. The data between the two transitions were also fit with a Curie–Weiss law, and an effective moment of $0.57\,\mu_B$ was calculated. The Weiss constant obtained in this case is $\theta = -17$ K again suggesting AFM interactions. The magnetic moment evaluated from the two temperature region fits indicates that the cobalt ions could be in low spin configuration in this compound. After the transition at 120 K the susceptibility drops substantially and a small cusp is seen at approximately 95 K. The magnetization

versus magnetic field (M vs. H) data recorded at 5, 100 and 170 K (the inset in Fig. 7) show a linear dependence for all three temperatures. Thus, the hysteresis data support the fact that the transitions observed in $Sr_3Co_2O_{5.38}$ in the ZFC/FC measurements are due to AFM ordering.

The susceptibility data for $Sr_3Co_2O_{5.64}$ as a function of temperature, and M vs. H curves at various temperatures, are presented in Figs. 8 and 9 respectively. The transition seen at 188 K in the ZFC/FC data indicates AFM interactions. After the magnetic transition, the susceptibility drops substantially with a large difference between ZFC and FC curves. The M vs. H data recorded at 5, 100 and 170 K indicate a very small hysteretic region that actually opens at 170 K. It can be concluded that the transition observed in this compound is primarily AFM but it also has a ferromagnetic (FM) component.

The magnetic data in constant field for $Sr_3Co_2O_{5.91}$ are shown in Fig. 10. Two magnetic transitions are observed for this compound: one at 225 K and another at 155 K. The magnitude of the transition at 155 K is almost $3\times$ higher than that of the transition at 225 K. A difference between ZFC and FC data is seen below the high temperature transition and the difference becomes very large below the low temperature transition precisely below 125 K. The divergence of ZFC and FC curves at low temperature for this compound is much higher, $\sim 5\times$, than the one observed in $Sr_3Co_2O_{5.64}$. The M vs. H data are recorded at 5, 100, 170, 210 and 225 K. A linear dependence of the magnetization with the field is observed at 210 and 225 K and this indicates that the transition at 225 K observed in constant field has AFM character. At lower temperatures, 5, 100 and 170 K, a loop opens up, and becomes largest at 100 K (Fig. 11). The features of the loop at 100 K suggest that some metamagnetism could also be present. The loop then closes again at lower temperature (see 5 K data in the Fig. 11). These data indicate that the transition at 155 K observed in constant filed involves FM interactions as indicated by the ZFC/FC data.

Similar magnetic behavior has been reported in other systems containing mixtures of Co^{2+}/Co^{3+} ions. For $Bi_2Sr_2Co_{6+\delta}$ ($0.23 \leqslant \delta \leqslant 0.5$), for instance [26], it was found that the system changes from AFM insulator to FM insulator as δ is reduced from ~0.5 to ~0.25. Thus, for oxygen-rich materials ($\delta > 0.4$) where the cobalt ions are mostly Co^{3+}, the system displays AFM long-range ordering. If δ is close to 0.25 the material has an approximately equal number of Co^{2+} and Co^{3+} and exhibits ferromagnetic behavior with $T_C \sim 100$ K. For intermediate values of δ, both AFM and FM domains were found. The domains represent clusters of equal numbers of Co^{2+} and Co^{3+} ferromagnetically coupled within an antiferromagnet formed by the Co^{3+} ions. The compounds in our study also have both Co^{2+} and Co^{3+}, with an increase in oxygen content resulting in increasing Co^{3+} ion concentration. However, unlike $Bi_2Sr_2CoO_{6+\delta}$, as the Co^{3+} concentration rises, the FM component is enhanced. The magnetic behavior of these compounds is clearly complex. Neutron diffraction studies at low temperatures would be needed to clarify the nature of their magnetism.

Fig. 12 shows the resistivity data for $Sr_3Co_2O_{5.91}$ from 290 to 210 K (the temperature range of the measurement was limited by the high value of the sample resistivity below 210 K). The resistivity increases rapidly with decreasing temperature and the data obeys a simple activated behavior (shown on inset), $\rho = \rho_0 \exp(E_a/kT)$, with an activation energy E_a of 0.23 eV. This value indicates that this compound is a semiconductor. Both $Sr_3Co_2O_{5.38}$ and $Sr_3Co_2O_{5.64}$ were too resistive and thus could not be measured by standard methods.

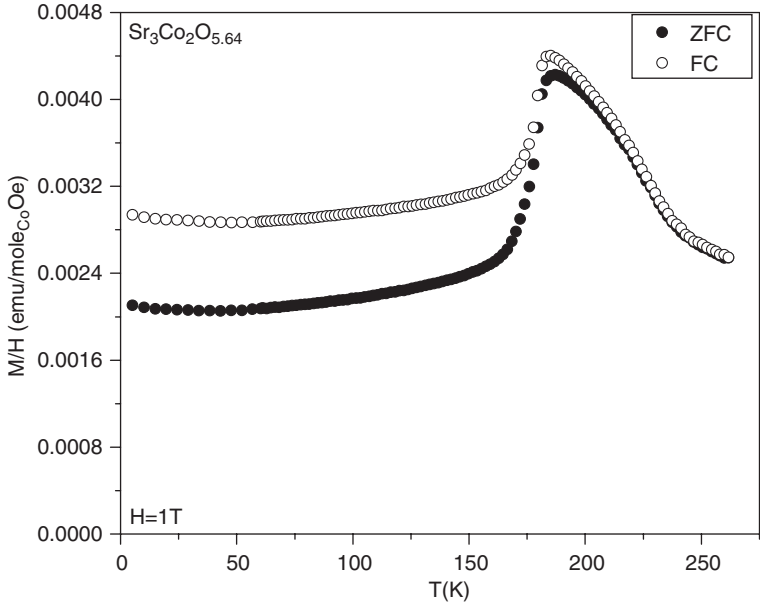

Fig. 8. Temperature dependence of magnetic susceptibility for $Sr_3Co_2O_{5.64}$.

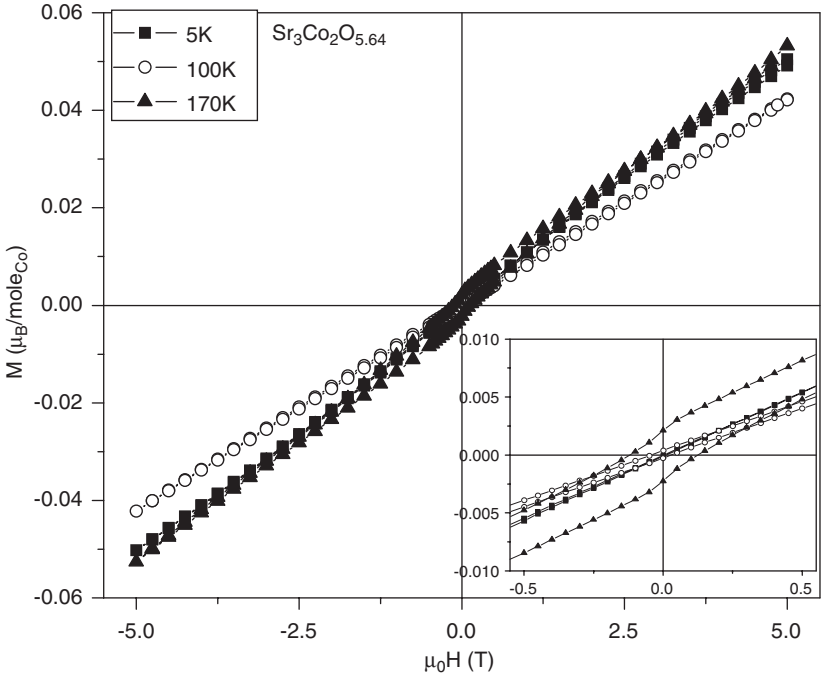

Fig. 9. Field dependence of the magnetization for $Sr_3Co_2O_{5.64}$. The inset shows a detail of the data between −0.5 and 0.5 T.

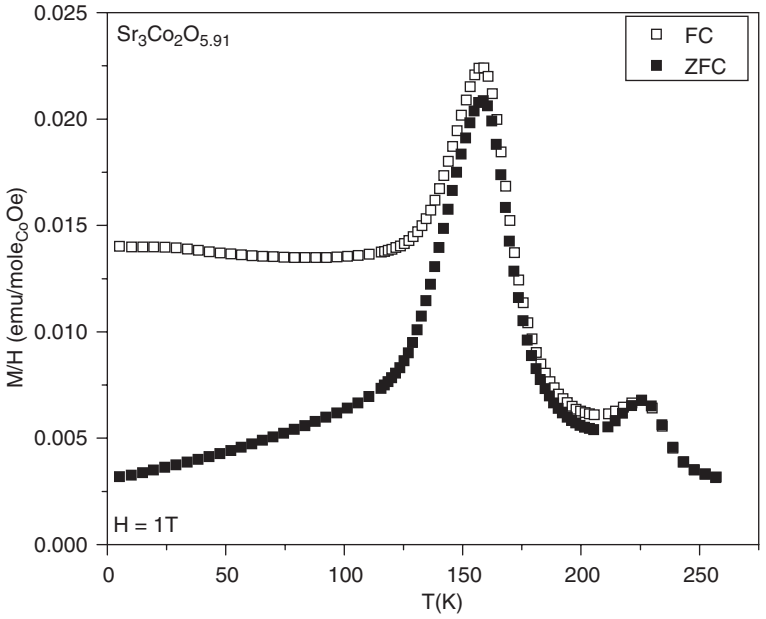

Fig. 10. Temperature dependence of magnetic susceptibility for $Sr_3Co_2O_{5.91}$.

The magnetic behavior of the sample treated with oxygen and exposed to moisture to form the hydroxyhydrated phase $Sr_3Co_2O_5(OH)_{1.2} \cdot 1.2(H_2O)$ was also investigated. The susceptibility data (ZFC and FC) recorded in an applied field of 1 T are presented in Fig. 13. The broad maximum developed between 50 and 80 K in the ZFC and FC data both suggest that there is a ferromagnetic component existent in the magnetic ordering of this material. Magnetization versus magnetic field data recorded at 5 and 65 K (the temperature where the maximum is found in the ZFC data) show hysteresis loops in both cases (Fig. 14) and support the data obtained in constant field. Unlike the magnetic data reported by Pelloquin et al. for nominally the same compound [24], the M vs. H loop in the present study has a small step at both temperatures, indicating a metamagnetic transition, and the magnetization value is almost ten times larger than is seen in their data. It may be that the magnetic properties of this

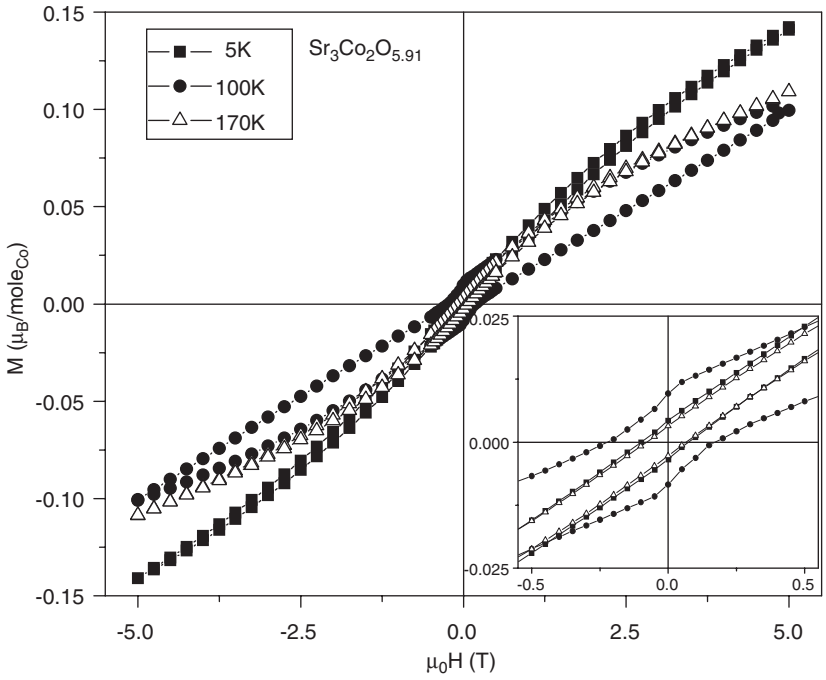

Fig. 11. Field dependence of the magnetization for $Sr_3Co_2O_{5.91}$. The inset shows a detail of the data between −0.5 and 0.5 T.

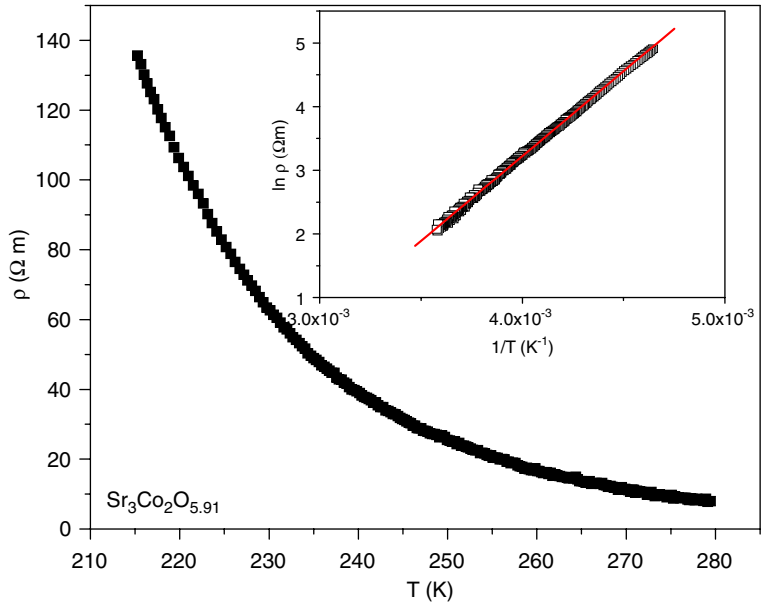

Fig. 12. Resistivity data for $Sr_3Co_2O_{5.91}$. The inset shows the linear fit of the ln ρ vs. temperature data.

compound are very strongly dependent on oxygen, hydroxyl, and water content.

4. Summary and conclusions

Three cobalt-based oxygen deficient members of an orthorhombic $Sr_3Co_2O_x$ ($x = 5 + \delta$) RP $n = 2$ compound were synthesized by solid-state reaction in an inert atmosphere. The structures of $Sr_3Co_2O_{5+\delta}$ with $\delta = 0.91$, 0.64 and 0.38 was determined via powder neutron diffraction and electron diffraction analysis. The oxygen vacancies are mainly found on the *b*-axis in the CoO_x plane, yielding a strong orthorhombic distortion. The magnetic measurements reveal complex behavior, with some ferromagnetic component to the ordering developed for $Sr_3Co_2O_{5.91}$ and $Sr_3Co_2O_{5.64}$. In attempts to increase the oxygen content, $Sr_3Co_2O_{6.06}$ is obtained, a material that is not stable in atmospheric conditions, converting to an oxyhydrated

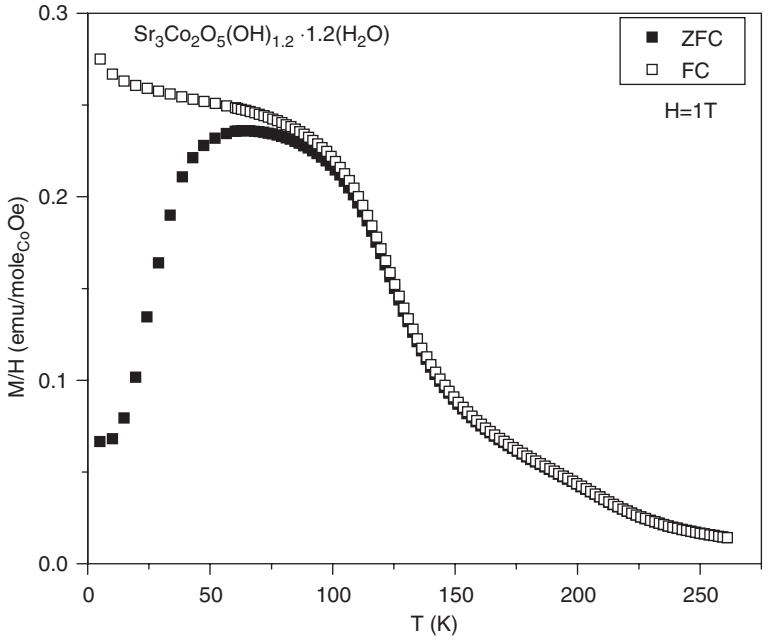

Fig. 13. Temperature dependence of magnetic susceptibility for $Sr_3Co_2O_5(OH)_{1.2} \cdot 1.2(H_2O)$.

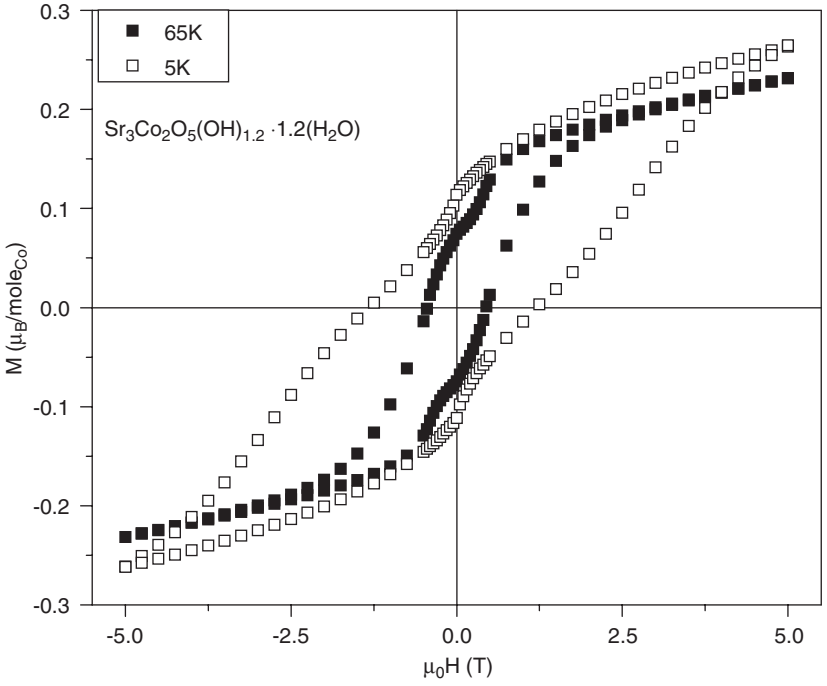

Fig. 14. Field dependence of the magnetization for $Sr_3Co_2O_5(OH)_{1.2} \cdot 1.2(H_2O)$.

form. Further study will be needed to determine the details of the magnetic behavior of these compounds. Although the spin state of the cobalt ions is not yet determined, these materials seem to be another example of RP-related solids with interesting competing magnetic phenomena. Additional tuning of the oxygen stoichiometry may be expected to provide even more diversity in both structure and properties that might be of interest from theoretical and experimental point of view.

Acknowledgments

This work was supported by the US Department of Energy, Grant DE-FG-02-ER45706, and by the NSF

MRSEC program, Grant DMR-0213706. The work at Delft was supported by The Nederlandse Stichting voor Fundamenteel Onderzoek der Materie (FOM).

References

[1] K. Takada, H. Sakurai, E. Takayama-Muromachi, F. Izumi, R.A. Dilanian, T. Sasaki, Nature 422 (2003) 53.
[2] R. Schaak, T. Klimczuk, M.L. Foo, R.J. Cava, Nature 424 (2003) 527.
[3] J.B. Goodenough, J. Phys. Chem. Solid 6 (1958) 287.
[4] A. Maignan, C. Martin, D. Pelloquin, N. Nguyen, B. Raveau, J. Solid State Chem. 142 (1999) 247.
[5] Y. Moritomota, T. Akimoto, M. Takio, A. Machida, E. Nishibori, M. Takata, M. Sakata, K. Ohoyama, A. Nakamura, Phys. Rev. B 61 (2000) R13325.
[6] H. Kusuya, A. Machida, Y. Moritomo, K. Kato, E. Nishibori, N. Takata, M. Sakato, A. Nakamura, J. Phys. Soc. Jpn. 70 (2001) 3577.
[7] S.E. Dann, M.T. Weller, B. Currie, J. Solid State Chem. 97 (1992) 179.
[8] K. Kuzushita, S. Morimoto, S. Nasu, S. Nakamura, J. Phys. Soc. Jpn. 69 (2000) 2767.
[9] H. Watanabe, T. Takeda, in: Y. Hashino, et al. (Eds.), Ferrites: Proceedings of the International Conference, July 1970, Tokyo University Press, Kyoto, Japan, 1971, p. 588.
[10] A. Nemudry, P. Rudolf, R. Schöllhorn, Chem. Mater. 8 (1996) 2232.
[11] J. Matsuno, Y. Okimoto, Z. Fang, X.Z. Yu, Y. Matsui, N. Nagaosa, M. Kawasaki, Y. Tokura, Phys. Rev. Lett. 93 (2004) 167202.
[12] S. Ghosh, P. Adler, Solid State Commun. 116 (2000) 585.
[13] F. Prado, A. Manthiram, J. Solid State Chem. 158 (2001) 307.
[14] Y. Bréard, C. Michel, A. Maignan, B. Raveau, Solid State Commun. 118 (2001) 517.
[15] S. Ghosh, P. Adler, J. Mater. Chem. 12 (2002) 511.
[16] Y. Bréard, C. Michel, M. Hervieu, F. Studer, A. Maignan, B. Raveau, Chem. Mater. 14 (2002) 3128.
[17] M. Abbate, L. Mogni, F. Prado, A. Caneiro, Phys. Rev. B 71 (2005) 195113.
[18] G.M. Veith, R. Chen, G. Popov, M. Croft, Y. Shokh, I. Nowik, M. Greenblatt, J. Solid State Chem. 166 (2002) 292.
[19] S.E. Dann, M.T. Weller, J. Solid State Chem. 115 (1995) 499.
[20] A. Larson, R.B. Von Dreele, GSAS: Generalized Structure Analysis System, Los Alamos National Laboratory, Los Alamos, NM, 1994.
[21] J.E. Huheey, E.A. Keiter, R.L. Keiter, Inorganic Chemistry, fourth ed., New York, 1993.
[22] N. McGlothlin, D. Ho, R.J. Cava, Mater. Res. Bull. 35 (2000) 1035; S.M. Loureiro, C. Felser, Q. Huang, R.J. Cava, Chem. Mater. 12 (2000) 3181.
[23] K. Boulahya, M. Parras, J.M. Gonzalez-Calbet, J. Solid State Chem. 145 (1999) 116.
[24] D. Pelloquin, N. Barrier, A. Maignan, V. Caignaert, Solid State Sci. 7 (2005) 853.
[25] M. Matvejeff, M. Lehtimaki, A. Hirasa, Y.-H. Huang, H. Yamauchi, M. Karppinen, Chem. Mater. 17 (2005) 2775.
[26] K.J. Thomas, Y.S. Lee, F.C. Chou, B. Khaykovich, P.A. Lee, M.A. Kastner, R.J. Cava, J.W. Lynn, Phys. Rev. B 66 (2002) 054415.